AGU PUBLICATIONS

JGR

Journal of Geophysical Research: Atmospheres

RESEARCH ARTICLE
10.1002/2014JD021712

Key Points:
- Examination of water vapor entering the stratosphere
- We show that it is controlled by four factors
- We see no trends in water entering the stratosphere

Correspondence to:
A. E. Dessler,
adessler@tamu.edu

Citation:
Dessler, A. E., M. R. Schoeberl, T. Wang, S. M. Davis, K. H. Rosenlof, and J.-P. Vernier (2014), Variations of stratospheric water vapor over the past three decades, *J. Geophys. Res. Atmos.*, *119*, 12,588–12,598, doi:10.1002/2014JD021712.

Received 4 MAR 2014
Accepted 31 OCT 2014
Accepted article online 5 NOV 2014
Published online 27 NOV 2014

Variations of stratospheric water vapor over the past three decades

A. E. Dessler[1], M. R. Schoeberl[2], T. Wang[1,3], S. M. Davis[4,5], K. H. Rosenlof[4], and J.-P. Vernier[6,7]

[1]Department of Atmospheric Sciences, Texas A&M University, Texas, USA, [2]Science and Technology Corporation, Columbia, Maryland, USA, [3]Jet Propulsion Laboratory, California Institute of Technology, Pasadena, California, USA, [4]NOAA Earth System Research Laboratory, Boulder, Colorado, USA, [5]Cooperative Institute for Research in Environmental Sciences, University of Colorado, Boulder, Colorado, USA, [6]Science Systems and Applications, Inc., Hampton, Virginia, USA, [7]NASA Langley Research Center, Hampton, Virginia, USA

Abstract We examine variations in water vapor in air entering the stratosphere through the tropical tropopause layer (TTL) over the past three decades in satellite data and in a trajectory model. Most of the variance can be explained by three processes that affect the TTL: the quasi-biennial oscillation, the strength of the Brewer-Dobson circulation, and the temperature of the tropical troposphere. When these factors act in phase, significant variations in water entering the stratosphere are possible. We also find that volcanic eruptions, which inject aerosol into the TTL, affect the amount of water entering the stratosphere. While there is clear decadal variability in the data and models, we find little evidence for a long-term trend in water entering the stratosphere through the TTL over the past 3 decades.

1. Introduction

Most of the air entering the stratospheric overworld (that part of the stratosphere at potential temperatures above 380 K [*Hoskins*, 1991]) travels through the tropical tropopause layer (TTL), where cold temperatures provide the primary control over its humidity [*Brewer*, 1949; *Fueglistaler et al.,* 2009]. Variations in the specific humidity of overworld air can therefore be traced to variations in TTL temperatures (following *Dessler et al.* [2013], we refer to the humidity of air entering the overworld as $H_2O_{ov\text{-}entry}$). The most dramatic variations in $H_2O_{ov\text{-}entry}$ are in response to the annual cycle in TTL temperatures, which generates an annual cycle in $H_2O_{ov\text{-}entry}$ of 2–3 parts per million by volume (ppmv) [*Mote et al.,* 1996].

Interannual variations in $H_2O_{ov\text{-}entry}$ are smaller than annual changes but are important for both climatic [*Forster and Shine*, 1999; *Solomon et al.,* 2010] and chemical [*Kirk-Davidoff et al.,* 1999] reasons. Previously investigated drivers of $H_2O_{ov\text{-}entry}$ variations include the quasi-biennial oscillation (QBO) [*Giorgetta and Bengtsson*, 1999; *Geller et al.,* 2002; *Randel et al.,* 2000; *Fueglistaler and Haynes*, 2005] and interannual variations in the strength of the Brewer-Dobson circulation (BDC) [*Randel et al.,* 2006; *Dhomse et al.,* 2008]. More recently, *Dessler et al.* [2013], hereafter D13, demonstrated a connection between interannual variations in tropospheric temperatures (ΔT) and $H_2O_{ov\text{-}entry}$ and used this to argue for the existence of a stratospheric water-vapor climate feedback. It has also been argued that volcanic eruptions may alter $H_2O_{ov\text{-}entry}$ [*Joshi and Shine*, 2003; *Fueglistaler*, 2012].

In addition to annual and interannual variations, the long-term trends in $H_2O_{ov\text{-}entry}$ could also be important, but they are not well quantified. Virtually all climate models predict that $H_2O_{ov\text{-}entry}$ will increase in the coming century [*Gettelman et al.,* 2010], and several analyses of balloon observations over the past few decades have concluded that there is a positive trend in $H_2O_{ov\text{-}entry}$ [*Oltmans and Hofmann*, 1995; *Oltmans et al.,* 2000; *Rosenlof et al.,* 2001; *Hurst et al.,* 2011], although other analyses [*Scherer et al.,* 2008; *Hegglin et al.,* 2014] have not found evidence of a long-term trend.

In this paper, we extend D13 by studying variations in $H_2O_{ov\text{-}entry}$ over the last few decades using measurements from satellite-borne instruments and from simulations from a trajectory model. We find that variations in QBO, BDC, and ΔT can explain most of the variance in $H_2O_{ov\text{-}entry}$ in both the observations and trajectory models. We also confirm that volcanic eruptions alter $H_2O_{ov\text{-}entry}$. Finally, we find little evidence that $H_2O_{ov\text{-}entry}$ has increased over the last few decades.

2. Data

2.1. Satellite Data

We analyze water vapor measurements from the Stratospheric Aerosol and Gas Experiment II (SAGE II) [*Thomason et al.,* 2004], the Halogen Occultation Experiment (HALOE) [*Harries et al.,* 1996], and the Aura Microwave Limb Sounder (MLS) [*Read et al.,* 2007]. The data sets and procedures we used to process them are described in the Appendix A. We focus on 82 hPa (~17.5 km altitude), monthly average, tropical interannual anomalies (in parts per million with respect to volume, ppmv). This is just above the tropical tropopause, and the water vapor abundance here is approximately equal to $H_2O_{ov\text{-}entry}$ because this air has just entered the stratosphere and little methane oxidation has taken place within it (owing to methane's long lifetime in the lower stratosphere, O(100 years) [e.g., *Dessler*, 2000, Figure 4.2]). All tropical averages in this paper cover 30°N–30°S, and interannual anomalies are calculated by subtracting off the data set's mean annual cycle.

2.2. Trajectory Model

We also estimate lower-stratospheric H_2O using a domain-filling forward trajectory model [*Schoeberl and Dessler*, 2011; *Schoeberl et al.,* 2012, 2013, hereafter SD11, S12, and S13, respectively]. In the version of the model analyzed here, an ensemble of 1350 parcels is initialized every day on an equal-area grid that spans all longitudes and runs from 60°S to 60°N, giving it a resolution of 3–5° latitude by 8° longitude. The parcels are initialized at 370 K potential temperature (~16 km), which is above the level of zero net radiative heating in the tropics (~355–360 K) but below the tropical tropopause (~375–380 K). Each parcel is run forward for either 15 years or until the parcel descends back into the troposphere, defined as reaching pressures above 250 hPa.

The model uses the Bowman trajectory code [*Bowman*, 1993; *Bowman and Carrie*, 2002], driven by 6-hourly instantaneous horizontal winds and 6-hourly average diabatic heating rates from the Modern Era Retrospective-Analysis for Research and Applications (MERRA) [*Rienecker et al.,* 2011] or ECMWF (European Centre for Medium-Range Weather Forecasts) interim reanalysis [*Dee et al.,* 2011] (ERAi).

Each trajectory is initialized with a water vapor mixing ratio of 50 ppmv. The mixing ratio is conserved along each trajectory, except when the relative humidity of the parcel exceeds 100%. In that case, excess water vapor is removed to prevent supersaturation. Despite the simplicity of this model, it has demonstrated the ability to accurately simulate stratospheric water vapor [SD11, S12, and S13]. Methane is also carried with the parcel, and it is oxidized along the trajectory, and the water produced is added to the parcel, but, as described above, that process is unimportant for this study.

$H_2O_{ov\text{-}entry}$ is calculated in the trajectory simulations by averaging the H_2O mixing ratio of parcels between 75 and 91 hPa (16.8–18.5 km), similar to the MLS 82 hPa weighting function, and between 30°N and 30°S. We will refer to the anomalies from the trajectory model driven by MERRA and ERAi meteorological fields as the "MERRA trajectory" and "ERAi trajectory" anomalies, respectively.

The model also has parameterizations for convective moistening and unresolved gravity waves [SD11]. While these parameterizations can affect the amount of water vapor in the stratosphere, we find that they have little effect on the interannual anomalies, so we turn them off for these simulations. In addition, we can vary the supersaturation threshold for condensate formation [SD11], but we leave it at 100% for these analyses. Again, the choice of the saturation threshold has minimal impact on the anomalies predicted by the model.

3. Analysis

3.1. Comparison Between the Observations and the Trajectory Model

Figure 1 shows good agreement between the satellite measurements and the trajectory simulations. The best agreement is between the MLS data and the trajectory simulations, with correlation coefficients of 0.96 (vs. ERAi) and 0.99 (vs. MERRA). This is in accord with previous comparisons between our model and MLS observations [SD11, S12, and S13]. The SAGE II and HALOE comparisons are also good, although less so than the MLS comparison. The correlation coefficients with SAGE II are 0.85 (vs. ERAi) and 0.88 (vs. MERRA); the HALOE correlation coefficients are 0.71 (vs. ERAi) and 0.75 (vs. MERRA).

The slightly worse performance of HALOE and SAGE II is not unexpected and has been seen in other analyses [*Fueglistaler et al.,* 2013]. HALOE and SAGE II are solar occultation measurements, and these instruments are more susceptible to interference from aerosols, such as after the 1991 eruption of Mt. Pinatubo [*Harries et al.,* 1996]. This

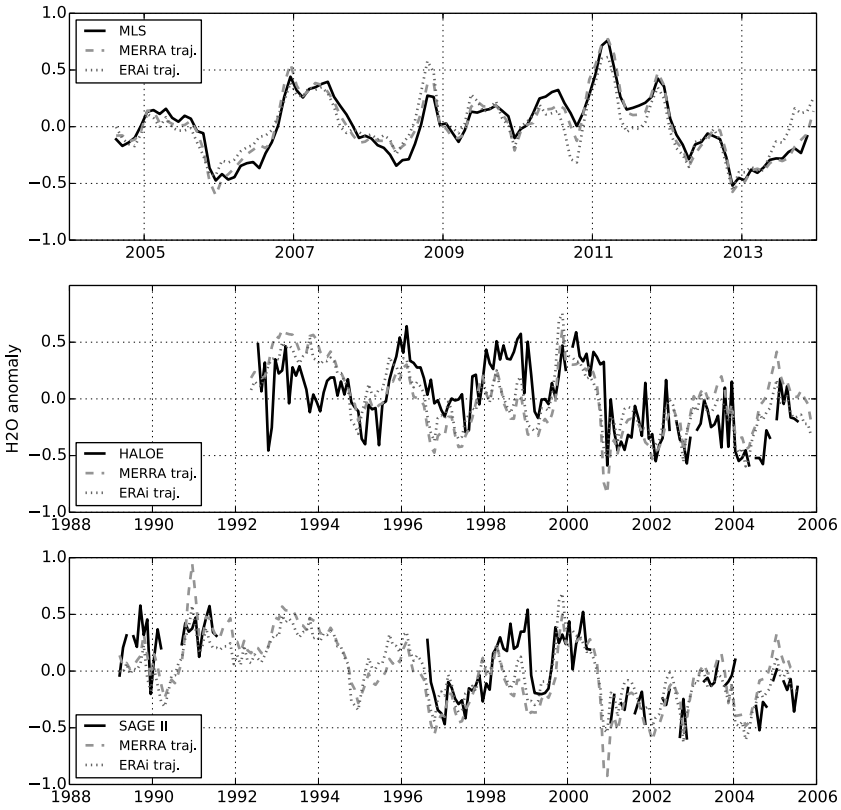

Figure 1. Monthly averaged tropical (30°N–30°S) lower-stratospheric (82 hPa, ~17.5 km) water vapor mixing ratio anomalies (in ppmv). Each panel contains one satellite data set, as indicated by the legend. Anomalies are calculated relative to the data set's full observation period. Each panel also contains the Modern Era Retrospective-Analysis for Research and Applications (MERRA) and European Centre for Medium-Range Weather Forecasts interim reanalysis (ERAi) trajectory simulations over the satellites' observation period. The trajectory simulations underlying each panel are the same, but the anomalies may differ because they are calculated relative the corresponding satellite's observation period.

is why much of the data in the early 1990s in the HALOE and SAGE II records are flagged as bad data (and are therefore missing in Figure 1). The MLS, on the other hand, measures in the microwave, making it less sensitive to stratospheric aerosol variations, and in any event the MLS has been observing during a period of low stratospheric aerosol abundances. Additionally, solar occultation measurements have sparse sampling, with each month having just 50–200 tropical measurements in it. The MLS, on the other hand, is an emission limb-sounder and makes ~30,000 tropical observations per month, leading to more precise and representative tropical averages.

Another possibility is that the reanalysis meteorological fields are better during the MLS period than earlier times because of the availability of more and better measurements to assimilate [e.g., *Fueglistaler et al.,* 2013]. This would lead to improvements in the reanalysis fields and better agreement between the trajectory models and MLS. Deficiencies in the reanalyses seem particularly likely for certain time periods (e.g., 1998–1999) because the trajectory calculations show similar differences to both HALOE and SAGE II measurements.

Overall, the excellent agreement between the trajectory model and the MLS data provides confidence in the trajectory model's simulations of $H_2O_{ov\text{-}entry}$ anomalies. One concern not addressed by the MLS data comparison is the potential that spurious long-term trends in the reanalysis meteorological fields could introduce spurious long-term trends in the trajectory simulations' H_2O_{entry} [e.g., *Bengtsson et al.,* 2004]. However, the quite reasonable long-term agreement between the trajectory simulations and the HALOE and SAGE II time series in Figure 1 argues against this being a significant problem.

3.2. Causes of the Variability of Stratospheric Water Vapor

The last section demonstrated that TTL temperature variations, as incorporated into the trajectory model, do a good job explaining interannual variations in $H_2O_{ov\text{-}entry}$. To better understand the sources of interannual

temperature and $H_2O_{ov\text{-}entry}$ variations, we regress the satellite observations and trajectory simulations of $H_2O_{ov\text{-}entry}$ against indices for the processes that we expect to control $H_2O_{ov\text{-}entry}$ using the regression model of D13:

$$H_2O_{ov\text{-}entry} = a\ \ QBO + b\ \ BDC + c\ \ \Delta T + r \quad (1)$$

For $H_2O_{ov\text{-}entry}$, we use 82 hPa tropical and monthly average H_2O mixing ratio anomalies. QBO is a quasi-biennial oscillation index, for which we use the standardized anomaly of monthly and zonally averaged equatorial 50 hPa winds (obtained from the NOAA Climate Prediction Center, http://www.cpc.ncep.noaa.gov/data/indices); BDC is a Brewer-Dobson circulation index (basically the strength of the vertical motion field), for which we use the tropical 82 hPa total heating rate anomaly as a surrogate. Heating rates come directly from the reanalyses; see *Wright and Fueglistaler* [2013] for details about those calculations. ΔT is the tropical average 500 hPa temperature anomaly, which represents the temperature of the tropical troposphere. D13 showed that this variable played an important role in the regression, although the physical mechanism was not identified.

We do not include the tropical tropopause temperature as one of the regressors because we consider it to be a response to the regressors that we do include. We also note that ENSO is an important driver of interannual climate variability and affects tropopause temperature; our tropical tropospheric temperature regressor captures most of that variability, so it is implicitly included in the fit. We discuss this point further below.

The QBO, BDC, and ΔT regressors are uncorrelated at the 95%-confidence level over the period 1980–2013. In the regression, they are lagged by 3, 1, and 3 months, respectively, to account for the finite time it takes for the change in the indices to impact TTL temperatures and then to be felt at 82 hPa. The exact lags are selected to maximize the explained variance, but each one is also physically plausible. For example, it takes a few months for the QBO signal to descend from 50 to 85 hPa and influence temperature. For the BDC, the temperature response to the diabatic heating is controlled by the local thermodynamic equation, which predicts a phase lag between BDC variations and TTL temperatures. Upper tropospheric response to anomalies such as the El Nino-Southern Oscillation (ENSO) lags the mid-troposphere by about 2 months which explains our time lag for the mid-tropospheric temperatures [*Scherllin-Pirscher et al.,* 2012].

For each satellite time series, we perform the regression twice, once using ΔT and BDC indices from the MERRA reanalysis and again using those indices from the ERAi reanalyses. The MLS and the trajectory model time series are regressed over the MLS time period (mid-2004 through 2013). While the trajectory model calculation starts in 1980, doing the regression over the MLS period allows us to focus on the period where we expect the indices from the reanalyses to be the most reliable. The HALOE and SAGE II regressions cover each instrument's observation period. The uncertainty in the regression coefficients takes autocorrelation of the time series into account following *Santer et al.* [2000].

The results of the regressions are listed in Table 1. The R^2 statistic, a standard measure of explained variance, shows that the fits to the two trajectory models and the MLS data are remarkably good, with R^2 of 0.7–0.8. Regressions of the HALOE and SAGE II observations have lower R^2 values and much larger coefficient uncertainty, likely because of uncertainties in the observations or errors in the ERAi or MERRA indices used in the regression. Nevertheless, the coefficients from the HALOE and SAGE II regressions are consistent with the trajectory and MLS regressions. Overall, we view the HALOE and SAGE II regressions as qualitatively confirming the MLS and trajectory model results but with limited quantitative usefulness, so we do not analyze them further in this study.

H_2O from MLS and $H_2O_{ov\text{-}entry}$ from the trajectory models, along with $H_2O_{ov\text{-}entry}$ reconstructed from the fits, are plotted in Figure 2, and they confirm that the fits are excellent. Note that the regressions of the trajectory models are performed over the MLS period, mid-2004–2013, and the coefficients derived over that period are then used with indices covering 1980–2013 to reconstruct H_2O over that entire period in Figure 2. The good agreement throughout the time period suggests that the regression coefficients are constant over this period. The clear exception is during the few years after volcanic eruptions in 1982 and 1991, both of which loaded the TTL and lower stratosphere with aerosols. The implication is that aerosols alter the relationship between the QBO, BDC, ΔT, and $H_2O_{ov\text{-}entry}$, with $H_2O_{ov\text{-}entry}$ being higher than predicted by the fit during times of high TTL aerosol. This is consistent with previous suggestions that volcanic eruptions would increase $H_2O_{ov\text{-}entry}$ by warming the tropopause [*Joshi and Shine*, 2003].

Table 1. Coefficients From Fits to $H_2O_{ov\text{-}entry}$ Time Series[a]

	Modern Era Retrospective-Analysis for Research and Applications (MERRA) traj	European Centre for Medium-Range Weather Forecasts interim reanalysis (ERAi) traj	Microwave Limb Sounder (MLS)/MERRA	MLS/ERAi	Halogen Occultation Experiment (HALOE)/MERRA	HALOE/ERAi	Stratospheric Aerosol and Gas Experiment II (SAGE II)/MERRA	SAGE II/ERAi
Regression period	2004–2014	2004–2014	2004–2014	2004–2014	1992–2005	1992–2005	1989–2005	1989–2005
Quasi-biennial oscillation (QBO)	0.10 +/− 0.05	0.09 +/− 0.03	0.12 +/− 0.05	0.11 +/− 0.04	0.06 +/− 0.10	0.04 +/− 0.08	0.02 +/− 0.12	0.03 +/− 0.10
Brewer-Dobson circulation (BDC)	−4.25 +/− 1.40	−2.48 +/− 0.55	−3.48 +/− 1.62	−2.51 +/− 0.83	−2.26 +/− 2.47	−2.43 +/− 1.35	−3.84 +/− 3.13	−2.92 +/− 1.63
Tropospheric temperature (ΔT)	0.18 +/− 0.17	0.17 +/− 0.11	0.30 +/− 0.20	0.34 +/− 0.17	0.18 +/− 0.35	0.22 +/− 0.28	0.11 +/− 0.33	0.17 +/− 0.28
R^2	0.74	0.79	0.72	0.75	0.15	0.29	0.25	0.36

[a]For the satellite observations, fits are calculated using both MERRA and ERAi for the BDC and ΔT indices. Also indicated are the time periods over which the fit is calculated. Uncertainties are 95%-confidence intervals. Units of the QBO, BD, and ΔT coefficients are ppmv, ppmv/(K/day), and ppmv/K, respectively.

The trajectory model regressions are insensitive to time period as long as the period does not include the high-aerosol aftermath of volcanic eruptions. If the regressions are performed over a period that includes one or both eruptions, we obtain similar coefficients for QBO and BDC, but much smaller coefficients for ΔT. This is unsurprising given that Figure 2 shows that the fit does a poorer job during the volcanic periods, so including those periods will degrade the results of the regression.

Figure 3 compares the MLS and trajectory coefficients graphically. For the QBO coefficients (Figure 3a), there is a good agreement between the regressions, with each yielding a value close to 0.1 ppmv. For the BDC coefficients, we see that $H_2O_{ov\text{-}entry}$ and the strength of the BDC are anticorrelated, as expected from the anti-correlation between TTL temperatures and the BDC strength [*Yulaeva et al.,* 1994]. The ERAi heating rates in the TTL are larger than those in MERRA, leading to smaller BDC coefficients in the ERAi regressions. See S12, *Wright and Fueglistaler* [2013], and *Wang et al.* [2014] for a more detailed discussion of these heating rates and their effects on the trajectory modeling of H_2O and tracers. Besides the direct impact on the BDC coefficient, the difference in heating rates has little other impact on our analysis. Overall, despite the differences in the regression coefficients (in Table 1), the time series reconstructed from the fits (including HALOE and SAGE II fits) are highly correlated to each other, with all correlation coefficients greater than 0.83 and most greater than 0.9.

The MLS and trajectory regressions also yield a positive coefficient for the ΔT index (Figure 3c), a result also found by D13, who used this to argue for the existence of a stratospheric water vapor feedback. There are differences among the regressions—in particular, the trajectory model regressions yield smaller ΔT coefficients than the MLS regressions, although the differences are not statistically significant. If this difference turns out to be real, it would suggest that the coupling of ΔT to $H_2O_{ov\text{-}entry}$ is not entirely through TTL temperatures [*Dessler et al.,* 2007; *Fueglistaler*, 2012]. An example of such a mechanism would be a warmer troposphere leads to enhanced convection and ice being lofting directly to the lower stratosphere, where the ice evaporates [*Rosenlof and Reid*, 2008]. This process would increase $H_2O_{ov\text{-}entry}$ without requiring a corresponding increase in TTL temperatures, and it would also help explain the large amount of heavy water, HDO, in the stratosphere [e.g., *Moyer et al.,* 1996; *Keith*, 2000; *Dessler et al.,* 2007; *Steinwagner et al.,* 2010].

Figure 4 shows the contribution of each regressor in the MLS and MERRA trajectory regressions. The peak-to-peak magnitude of the QBO component is ~0.3 ppmv, consistent with previous studies [*Giorgetta and Bengtsson*, 1999; *Geller et al.,* 2002; *Randel et al.,* 2000; *Fueglistaler and Haynes*, 2005]; the magnitude of the BDC component is ~0.4–0.6 ppmv. When these two processes are in phase, large changes in $H_2O_{ov\text{-}entry}$ can occur. A good example is the drop in $H_2O_{ov\text{-}entry}$ in 2000 (i.e., see the top panel of Figure 2)—our analysis agrees with previous work [*Randel et al.,* 2006; *Dhomse et al.,* 2008; *Fueglistaler*, 2012] that a major cause was a change in

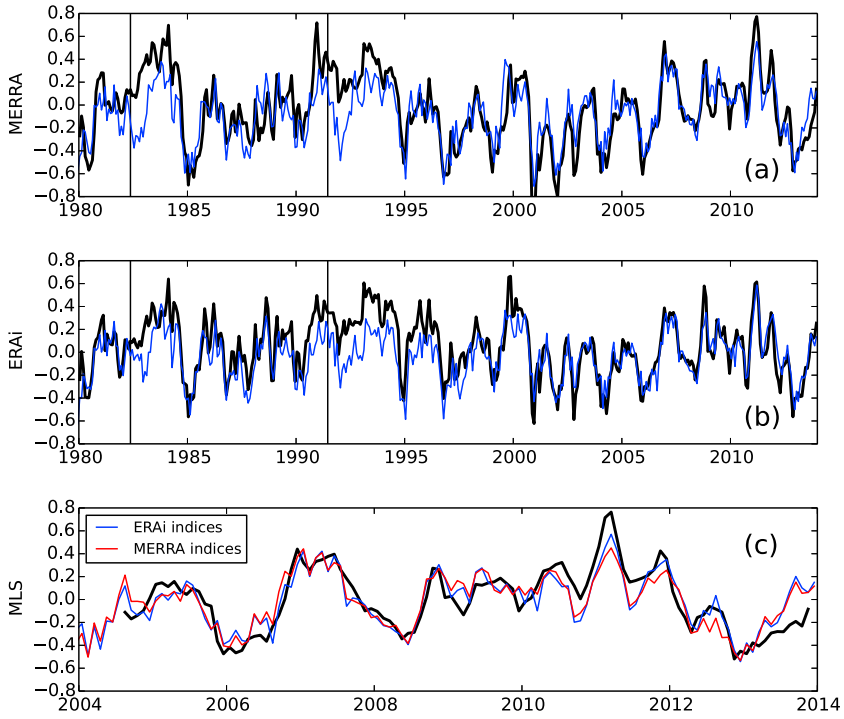

Figure 2. Time series of monthly averaged tropical 82 hPa H_2O anomalies (in ppmv). Figures 2a and 2b show the MERRA and ERAi trajectory calculations (black lines), as well as fits to those time series (blue lines). The vertical lines in these panels indicate the dates of major tropical volcanic eruptions. Figure 2c shows Microwave Limb Sounder (MLS) measurements (black line), along with the fits using MERRA (red) and ERAi regressors (blue).

the BDC. We also see, however, that there was also a contribution from QBO cooling of the tropopause at the same time the BDC cooled the tropopause. Another large drop occurred in 2012 [*Urban et al.,* 2014], similarly caused by combined BDC and QBO variations.

Finally, we see that the ΔT term introduces variations as large as 0.4 ppmv, and it clearly shows the $H_2O_{ov\text{-}entry}$ response to warming from ENSO events in 1987, 1998, and 2010; the connection between ENSO and $H_2O_{ov\text{-}entry}$ has been previously discussed [e.g., *Geller et al.,* 2002]. Given that most of the ΔT variability is due to ENSO, one might reasonably wonder whether the fundamental control on $H_2O_{ov\text{-}entry}$ is the tropical tropospheric average temperature, which is what we used in our regression, or another aspect of ENSO, such as the rearrangement in tropospheric circulation.

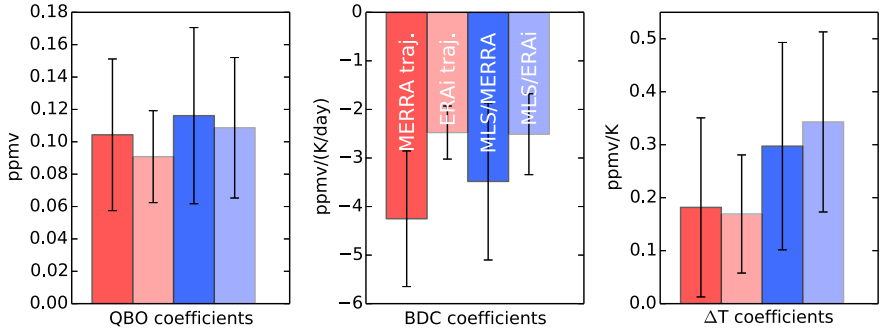

Figure 3. Graphical comparison of coefficients from the regressions. Each panel compares the coefficients for one variable from the trajectory and MLS regressions, along with 95%-confidence intervals. The trajectory results are regressed using indices from that same reanalysis, while the MLS data are regressed using indices from both reanalyses. Bars are labeled in the middle panel; the order of bars is the same in each panel. The numerical values plotted here are listed in Table 1.

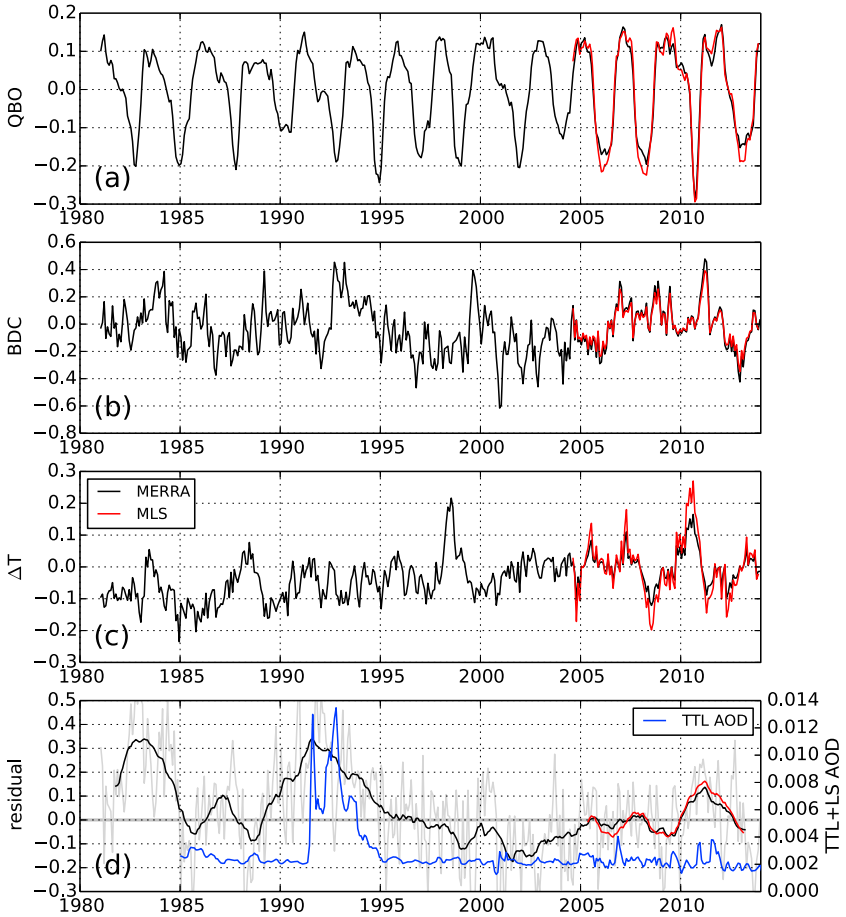

Figure 4. The variability of $H_2O_{ov\text{-}entry}$ from each regressor (in ppmv). Values are obtained from the regressions of the MERRA trajectory model and the MLS observations (using MERRA indices) and are equal to the coefficient for that regressor times that regressor index. The bottom panel plots the residuals ($H_2O_{ov\text{-}entry}$ minus fit). The light-gray line is the monthly residual from the trajectory model regression, while the black and red lines are residuals from the model and MLS smoothed with an 18 month running average. The blue line in the bottom panel is the aerosol optical depth in the TTL and lower stratosphere.

To address this question, we have re-calculated the regressions using the Nino3.4 index [*Trenberth*, 1997] in place of the ΔT time series (and using a range of lags). The R^2 of the ENSO fits are generally about 0.05–0.1 lower than fits using ΔT as a regressor. The R^2 of the ENSO fits are highest when the ENSO index is lagged by 7–10 months. This also happens to be the lag that maximizes the correlation of the Nino34 index with the ΔT regressor index. Thus, whatever physical process is responsible for this component of the regression correlates with tropical average tropospheric temperature ΔT. The most parsimonious conclusion is that it is the tropical average temperature itself that controls $H_2O_{ov\text{-}entry}$, and the $H_2O_{ov\text{-}entry}$ variations during ENSO are really a response to the ENSO-induced ΔT changes. Supporting this conclusion, climate models show a similar response of $H_2O_{ov\text{-}entry}$ to both short-term and long-term ΔT variations [D13, Table 1].

The residuals are plotted in Figure 4d, along with the monthly average integrated aerosol optical depth (AOD) from 15 to 20 km in the tropics (the data set is described in the Appendix A). During non-volcanic periods (low AOD), the smoothed residual is generally between ±0.1 ppmv. The residual does show potential geophysical structure, such as a the increase prior to eruption of Mt. Pinatubo [also noted by *Fueglistaler*, 2012] and the decadal increase from 2001 to 2013, which may indicate that factors not considered in equation (1) play a non-negligible role in determining $H_2O_{ov\text{-}entry}$.

The AOD also shows that the eruption of Mt. Pinatubo significantly increased aerosol surface area in the TTL and lower stratosphere. The residual of the fit is largest during that period as well as the period just after

the eruption of El Chichon. There is also a slight enhancement of AOD after 2010, along with a slight increase in the residual. During those periods, the fit underestimates $H_2O_{ov\text{-}entry}$. Thus, we conclude that volcanic injections of aerosols into the TTL and lower stratosphere affected $H_2O_{ov\text{-}entry}$ [*Joshi and Shine*, 2003; *Fueglistaler*, 2012].

There are several possible ways aerosols might do this. First, everything else being equal, aerosols are expected to warm the lower stratosphere [*Robock*, 2000; *Joshi and Shine*, 2003; *Free and Lanzante*, 2009], the region where final dehydration of air entering the stratosphere takes place. This will tend to increase stratospheric water vapor relative to non-volcanic periods, and that effect will not be reproduced by the fits. It is also possible that there are errors in the regressors during this time, particularly for the BDC index, since neither reanalysis assimilates aerosol data. The reanalyses handle ozone differently: while the MERRA uses prognostic ozone, ERAi uses an ozone climatology in its heating rate calculations [*Wright and Fueglistaler*, 2013]. The similarity of the MERRA and ERAi results, however, suggests that ozone variations are probably not an important component of the volcanic response.

3.3. Long-Term Trends

We estimate the long-term linear trend in $H_2O_{ov\text{-}entry}$ via linear least square fit of the two trajectory model runs from 1980 to 2014. Inspection of Figure 2 shows that the trend may be sensitive to the beginning and ending point selected, so we vary the beginning and ending point over the first and last decades of the time series. We obtain trends ranging from −0.14 ppmv/decade to +0.07 ppmv/decade; none of these trends are statistically different from zero.

Given the success of the regression in reproducing the observations, another approach is to calculate trends in the regressors (QBO, BD, and ΔT). We have again varied the beginning and endpoints of the trend calculation. The average trend in the QBO index is 0.005/decade; none of the QBO trends are statistically significant. The average trend in the BDC index is 0.011 K/day/decade, indicating a slight strengthening; about 13% of the trend calculations are statistically significant. Given that the climate is warming, we are not surprised to find that the ΔT regressor has statistically significant warming in 87% of the trends, and the average trend is 0.23 K/decade.

We can estimate the impact of the trends in BDC and ΔT on $H_2O_{ov\text{-}entry}$ trends by multiplying these trends by regression coefficients from Table 1. Using average coefficients of −3.2 ppmv/(K/day) and 0.25 ppmv/K, we estimate the BDC and ΔT trends lead to trends in $H_2O_{ov\text{-}entry}$ of −0.04 ppmv/decade and +0.06 ppmv/decade. These largely cancel out (as noted by D13), leaving a much smaller residual trend that is generally consistent with a total trend near zero.

Thus, we see no firm evidence of trends (either positive or negative) in $H_2O_{ov\text{-}entry}$ since the 1980s, in agreement with *Hegglin et al.* [2014]. It is possible of course that a trend does exist but is too small to identify given the large interannual and interdecadal variability. In addition, both the trajectory model and the regressors come from reanalyses, so spurious trends in the renalyses might obscure a real trend. On the other hand, the good agreement between the trajectory models and the HALOE and SAGE II observations in Figure 1 suggest that the long-term behavior of the reanalysis is reasonable.

4. Conclusions

We have used satellite observations of H_2O entering the stratosphere through the TTL ($H_2O_{ov\text{-}entry}$), along with simulations from a domain-filling forward trajectory model, to determine the factors that control $H_2O_{ov\text{-}entry}$. The trajectory simulations agree well with the various observational data sets covering the period from the mid 1980s to the early 2010s. This is consistent with previous trajectory model results [SD11, S12, and S13, *Fueglistaler et al.,* 2013].

Our analysis shows that the QBO and variations in the BDC and tropospheric temperatures can explain most of the variance in $H_2O_{ov\text{-}entry}$ over the past few decades. When in-phase, significant changes, such as the drop in $H_2O_{ov\text{-}entry}$ after 2000 and 2012, can occur. Regressions of the various $H_2O_{ov\text{-}entry}$ data sets suggest $H_2O_{ov\text{-}entry}$ increases with tropical tropospheric temperatures, supporting the existence of a stratospheric water vapor feedback [D13]. We also find that TTL aerosols from a large volcanic eruption can influence $H_2O_{ov\text{-}entry}$.

Analysis of the trajectory models and the observations show no clear trends since the mid-1980s. However, this conclusion is complicated by large decadal variability, possible spurious trends in the reanalysis meteorological fields, and effects of volcanic eruptions in the early 1980s and early 1990s.

Appendix A: Satellite Observations

The SAGE II is a solar occultation instrument that operated from October 1984 to August 2005 [*McCormick et al.,* 1989]. Here, we use version 7.0 data from SAGE II, which is an update from the prior version [version 6.2, *Thomason et al.,* 2004]. We exclude SAGE II water vapor data before 1 January 1986 due to a known drift in the water vapor channel filter parameters during this time period. SAGE II water vapor data are filtered according to the published recommendations of *Taha et al.* [2004] and *Rind et al.* [2005]. Specifically, we remove any points with water vapor uncertainty >50%. Additionally we remove all data in a profile below the highest altitude point at which either cloud presence is flagged or β_{1020} (1020 nm extinction) $>2\times10^{-4}\,\mathrm{km}^{-1}$ and all profiles associated with "short events" during 1993–1994, as described in *Taha et al.* [2004]. We also remove clearly unphysical values by eliminating mixing ratios above 30 ppmv and points farther than 3σ from the mean in 10° latitude bins.

The HALOE is another solar occultation instrument that operated from October 1991 until November 2005, making water vapor measurements in the infrared with latitudinal coverage from 80°S to 80°N [*Harries et al.,* 1996]. Here, we use the HALOE version 19 products, which have been extensively compared to independent satellite, balloon, and ground-based data [*Kley et al.,* 2000]. The HALOE data are filtered by removing any "trip angle" or "constant lockdown angle" events identified by the data providers (http://haloe.gats-inc.com/user_docs/index.php). Then, points with uncertainties ≥100% are removed.

The MLS [*Waters et al.,* 2006] was launched in July 2004 aboard NASA's Aura satellite and is still operating (knock on wood). The MLS measures thermally emitted microwave radiation from the Earth's limb, from which water vapor can be retrieved [*Read et al.,* 2007]. MLS obtains ~3500 profiles per day and achieves nearly global coverage between 82°S and 82°N. We use version 3.3 data and quality control the data following MLS' recommendations (http://mls.jpl.nasa.gov/data/v3-3_data_quality_document.pdf).

For all three satellite data sets, the tropical data are binned into 10°-latitude boxes and then averaged. These 10°-latitude averages are then averaged to come up with a tropical value. Because of the sparse sampling of the solar occultation measurements, not all 10° bins have values in them every month. We have used the trajectory model to test if the limited sampling of the solar occultation instruments biases or produces significant variability in the calculated tropical average anomaly time series and found that it does not.

The aerosol data in Figure 4 are monthly average integrated aerosol optical depth from 15 to 20 km in the tropics from 1985 to 2013 [*Vernier et al.,* 2011]. The time series is constructed from SAGE II, CALIPSO, GOMOS/ENVISAT, and OSIRIS/Odin observations. Between the June 1991 eruption of Mt Pinatubo and the end of 1993, a substantial part of the SAGE II data are missing in the TTL region due to complete attenuation of the solar signal. Lidar measurements from Mauna Loa (USA) and Camaguey (Cuba) have been used to fill those gaps, as described in *SPARC* [2006].

Acknowledgments
This work was supported by NSF grant AGS-1261948 and NASA grant NNX13AK25G, both to Texas A&M University. We thank Bernard Legras for help with the ERAi model runs. The quality-controlled satellite data, compiled in the SWOOSH data set, can be found at http://www.esrl.noaa.gov/csd/groups/csd8/swoosh/. The met fields used in the trajectory calculation can be found at http://data-portal.ecmwf.int/data/d/interim_daily/ and http://disc.sci.gsfc.nasa.gov/.

References

Bengtsson, L., S. Hagemann, and K. I. Hodges (2004), Can climate trends be calculated from reanalysis data?, *J. Geophys. Res.*, *109*, D11111, doi:10.1029/2004JD004536.

Bowman, K. P. (1993), Large-scale isentropic mixing properties of the Antarctic polar vortex from analyzed winds, *J. Geophys. Res.*, *98*, 23,013–23,027, doi:10.1029/93JD02599.

Bowman, K. P., and G. D. Carrie (2002), The mean-meridional transport circulation of the troposphere in an idealized GCM, *J. Atmos. Sci.*, *59*, 1502–1514.

Brewer, A. W. (1949), Evidence for a world circulation provided by the measurements of helium and water vapour distribution in the stratosphere, *Q. J. R. Meteorol. Soc.*, *75*, 351–363.

Dee, D. P., et al. (2011), The ERA-Interim reanalysis: Configuration and performance of the data assimilation system, *Q. J. R. Meteorol. Soc.*, *137*, 553–597, doi:10.1002/qj.828.

Dessler, A. E. (2000), *The Chemistry and Physics of Stratospheric Ozone*, 214 pp., Academic Press, San Diego, Calif.

Dessler, A. E., T. F. Hanisco, and S. Fueglistaler (2007), Effects of convective ice lofting on H_2O and HDO in the tropical tropopause layer, *J. Geophys. Res.*, *112*, D18309, doi:10.1029/2007JD008609.

Dessler, A. E., M. R. Schoeberl, T. Wang, S. M. Davis, and K. H. Rosenlof (2013), Stratospheric water vapor feedback, *Proc. Natl. Acad. Sci. U.S.A.*, *110*, 18,087–18,091, doi:10.1073/pnas.1310344110.

Dhomse, S., M. Weber, and J. Burrows (2008), The relationship between tropospheric wave forcing and tropical lower stratospheric water vapor, *Atmos. Chem. Phys.*, *8*, 471–480, doi:10.5194/acp-8-471-2008.

Forster, P. M. D., and K. P. Shine (1999), Stratospheric water vapour changes as a possible contributor to observed stratospheric cooling, *Geophys. Res. Lett.*, *26*, 3309–3312, doi:10.1029/1999GL010487.
Free, M., and J. Lanzante (2009), Effect of volcanic eruptions on the vertical temperature profile in radiosonde data and climate models, *J. Clim.*, *22*, 2925–2939, doi:10.1175/2008jcli2562.1.
Fueglistaler, S. (2012), Stepwise changes in stratospheric water vapor?, *J. Geophys. Res.*, *117*, D13302, doi:10.1029/2012JD017582.
Fueglistaler, S., and P. H. Haynes (2005), Control of interannual and longer-term variability of stratospheric water vapor, *J. Geophys. Res.*, *110*, D24108, doi:10.1029/2005JD006019.
Fueglistaler, S., A. E. Dessler, T. J. Dunkerton, I. Folkins, Q. Fu, and P. W. Mote (2009), The tropical tropopause layer, *Rev. Geophys.*, *47*, RG1004, doi:10.1029/2008RG000267.
Fueglistaler, S., et al. (2013), The relation between atmospheric humidity and temperature trends for stratospheric water, *J. Geophys. Res. Atmos.*, *118*, 1052–1074, doi:10.1002/jgrd.50157.
Geller, M. A., X. L. Zhou, and M. H. Zhang (2002), Simulations of the interannual variability of stratospheric water vapor, *J. Atmos. Sci.*, *59*, 1076–1085.
Gettelman, A., et al. (2010), Multimodel assessment of the upper troposphere and lower stratosphere: Tropics and global trends, *J. Geophys. Res.*, *115*, D00M08, doi:10.1029/2009JD013638.
Giorgetta, M. A., and L. Bengtsson (1999), Potential role of the quasi-biennial oscillation in the stratosphere-troposphere exchange as found in water vapor in general circulation model experiments, *J. Geophys. Res.*, *104*, 6003–6019, doi:10.1029/1998JD200112.
Harries, J. E., J. M. Russell III, A. F. Tuck, L. L. Gordley, P. Purcell, K. Stone, R. M. Bevilacqua, M. Gunson, G. Nedoluha, and W. A. Traub (1996), Validation of measurements of water vapor from the Halogen Occultation Experiment (HALOE), *J. Geophys. Res.*, *101*, 10,205–10,216, doi:10.1029/95JD02933.
Hegglin, M. I., et al. (2014), Vertical structure of stratospheric water vapour trends derived from merged satellite data, *Nat. Geosci.*, *7*, 768–776, doi:10.1038/ngeo2236.
Hoskins, B. J. (1991), Towards a PV-q view of the general circulation, *Tellus*, *43AB*, 27–35.
Hurst, D. F., S. J. Oltmans, H. Vomel, K. H. Rosenlof, S. M. Davis, E. A. Ray, E. G. Hall, and A. Jordan (2011), Stratospheric water vapor trends over Boulder, Colorado: Analysis of the 30 year Boulder record, *J. Geophys. Res.*, *116*, D02306, doi:10.1029/2010JD015065.
Joshi, M. M., and K. P. Shine (2003), A GCM study of volcanic eruptions as a cause of increased stratospheric water vapor, *J. Clim.*, *16*, 3525–3534, doi:10.1175/1520-0442(2003)016<3525:agsove>2.0.co;2.
Keith, D. W. (2000), Stratosphere-troposphere exchange: Inferences from the isotopic composition of water vapor, *J. Geophys. Res.*, *105*, 15,167–15,173, doi:10.1029/2000JD900130.
Kirk-Davidoff, D. B., E. J. Hintsa, J. G. Anderson, and D. W. Keith (1999), The effect of climate change on ozone depletion through changes in stratospheric water vapour, *Nature*, *402*, 399–401.
Kley, D., J. M. Russell III, and C. Phillips (Eds.) (2000), SPARC assessment of upper tropospheric and stratospheric water vapour, *WCRP-113, WMO/TD-No. 1043, SPARC Rep. No. 2*, World Climate Research Programme (WCRP).
McCormick, M. P., J. M. Zawodny, R. E. Veiga, J. C. Larsen, and P. H. Wang (1989), An overview of SAGE I and II ozone measurements, *Planet. Space Sci.*, *37*, 1567–1586.
Mote, P. W., K. H. Rosenlof, M. E. McIntyre, E. S. Carr, J. C. Gille, J. R. Holton, J. S. Kinnersley, H. C. Pumphrey, J. M. Russell III, and J. W. Waters (1996), An atmospheric tape recorder: The imprint of tropical tropopause temperatures on stratospheric water vapor, *J. Geophys. Res.*, *101*, 3989–4006, doi:10.1029/95JD03422.
Moyer, E. J., F. W. Irion, Y. L. Yung, and M. R. Gunson (1996), ATMOS stratospheric deuterated water and implications for troposphere-stratosphere transport, *Geophys. Res. Lett.*, *23*, 2385–2388, doi:10.1029/96GL01489.
Oltmans, S. J., and D. J. Hofmann (1995), Increase in lower-stratospheric water vapour at a mid-latitude northern hemisphere site from 1981 to 1994, *Nature*, *374*, 146–149.
Oltmans, S. J., H. Vömel, D. J. Hofmann, K. H. Rosenlof, and D. Kley (2000), The increase in stratospheric water vapor from balloonborne, frostpoint hygrometer measurements at Washington, D.C., and Boulder, Colorado, *Geophys. Res. Lett.*, *27*, 3453–3456, doi:10.1029/2000GL012133.
Randel, W. J., F. Wu, and D. J. Gaffen (2000), Interannual variability of the tropical tropopause derived from radiosonde data and NCEP reanalysis, *J. Geophys. Res.*, *105*, 15,509–15,523, doi:10.1029/2000JD900155.
Randel, W. J., F. Wu, H. Vomel, G. E. Nedoluha, and P. Forster (2006), Decreases in stratospheric water vapor after 2001: Links to changes in the tropical tropopause and the Brewer-Dobson circulation, *J. Geophys. Res.*, *111*, D12312, doi:10.1029/2005JD006744.
Read, W. G., et al. (2007), Aura Microwave Limb Sounder upper tropospheric and lower stratospheric H_2O and relative humidity with respect to ice validation, *J. Geophys. Res.*, *112*, D24S35, doi:10.1029/2007JD008752.
Rienecker, M. M., et al. (2011), MERRA - NASA's Modern-Era Retrospective Analysis for Research and Applications, *J. Clim.*, *24*, 3624–3648, doi:10.1175/JCLI-D-11-00015.1.
Rind, D., J. Lerner, and J. Zawodny (2005), A complementary analysis for SAGE II data profiles, *Geophys. Res. Lett.*, *32*, L07812, doi:10.1029/2005GL022550.
Robock, A. (2000), Volcanic eruptions and climate, *Rev. Geophys.*, *38*, 191–219, doi:10.1029/1998RG000054.
Rosenlof, K. H., and G. C. Reid (2008), Trends in the temperature and water vapor content of the tropical lower stratosphere: Sea surface connection, *J. Geophys. Res.*, *113*, D06107, doi:10.1029/2007JD009109.
Rosenlof, K. H., et al. (2001), Stratospheric water vapor increases over the past half-century, *Geophys. Res. Lett.*, *28*, 1195–1198, doi:10.1029/2000GL012502.
Santer, B. D., T. M. L. Wigley, J. S. Boyle, D. J. Gaffen, J. J. Hnilo, D. Nychka, D. E. Parker, and K. E. Taylor (2000), Statistical significance of trends and trend differences in layer-average atmospheric temperature time series, *J. Geophys. Res.*, *105*, 7337–7356, doi:10.1029/1999JD901105.
Scherer, M., H. Vomel, S. Fueglistaler, S. J. Oltmans, and J. Staehelin (2008), Trends and variability of midlatitude stratospheric water vapour deduced from the re-evaluated Boulder balloon series and HALOE, *Atmos. Chem. Phys.*, *8*, 1391–1402.
Scherllin-Pirscher, B., C. Deser, S. P. Ho, C. Chou, W. Randel, and Y. H. Kuo (2012), The vertical and spatial structure of ENSO in the upper troposphere and lower stratosphere from GPS radio occultation measurements, *Geophys. Res. Lett.*, *39*, L20801, doi:10.1029/2012GL053071.
Schoeberl, M. R., and A. E. Dessler (2011), Dehydration of the stratosphere, *Atmos. Chem. Phys.*, *11*, 8433–8446, doi:10.5194/acp-11-8433-2011.
Schoeberl, M. R., A. E. Dessler, and T. Wang (2012), Simulation of stratospheric water vapor and trends using three reanalyses, *Atmos. Chem. Phys.*, *12*, 6475–6487, doi:10.5194/acp-12-6475-2012.
Schoeberl, M. R., A. E. Dessler, and T. Wang (2013), Modeling upper tropospheric and lower stratospheric water vapor anomalies, *Atmos. Chem. Phys.*, *13*, 7783–7793, doi:10.5194/acp-13-7783-2013.

Solomon, S., K. H. Rosenlof, R. W. Portmann, J. S. Daniel, S. M. Davis, T. J. Sanford, and G. K. Plattner (2010), Contributions of stratospheric water vapor to decadal changes in the rate of global warming, *Science*, *327*, 1219–1223, doi:10.1126/science.1182488.

SPARC (2006), Assessment of stratospheric aerosol properties, *SPARC Rep. No. 4, WCRP-124, WMO/TD-No. 1295*, edited by L. Thomason and T. Peter.

Steinwagner, J., S. Fueglistaler, G. Stiller, T. von Clarmann, M. Kiefer, P. P. Borsboom, A. van Delden, and T. Rockmann (2010), Tropical dehydration processes constrained by the seasonality of stratospheric deuterated water, *Nat. Geosci.*, *3*, 262–266, doi:10.1038/ngeo822.

Taha, G., L. W. Thomason, and S. P. Burton (2004), Comparison of Stratospheric Aerosol and Gas Experiment (SAGE) II version 6.2 water vapor with balloon-borne and space-based instruments, *J. Geophys. Res.*, *109*, D18313, doi:10.1029/2004JD004859.

Thomason, L. W., S. P. Burton, N. Iyer, J. M. Zawodny, and J. Anderson (2004), A revised water vapor product for the Stratospheric Aerosol and Gas Experiment (SAGE) II version 6.2 data set, *J. Geophys. Res.*, *109*, D06312, doi:10.1029/2003JD004465.

Trenberth, K. E. (1997), The definition of El Niño, *Bull. Am. Meteorol. Soc.*, *78*, 2771–2777, doi:10.1175/1520-0477(1997)078<2771:tdoeno>2.0.co;2.

Urban, J., S. Lossow, G. Stiller, and W. Read (2014), Another drop in water vapor, *Eos Trans. AGU*, *94*, 245–246, doi:10.1002/2014EO270001.

Vernier, J. P., et al. (2011), Major influence of tropical volcanic eruptions on the stratospheric aerosol layer during the last decade, *Geophys. Res. Lett.*, *38*, L12807, doi:10.1029/2011GL047563.

Wang, T., W. J. Randel, A. E. Dessler, M. R. Schoeberl, and D. E. Kinnison (2014), Trajectory model simulations of ozone (O3) and carbon monoxide (CO) in the lower stratosphere, *Atmos. Chem. Phys.*, *14*, 7135–7147, doi:10.5194/acp-14-7135-2014.

Waters, J. W., et al. (2006), The Earth Observing System Microwave Limb Sounder (EOS MLS) on the Aura satellite, *IEEE Trans. Geosci. Remote Sens.*, *44*, 1075–1092.

Wright, J. S., and S. Fueglistaler (2013), Large differences in reanalyses of diabatic heating in the tropical upper troposphere and lower stratosphere, *Atmos. Chem. Phys.*, *13*, 9565–9576, doi:10.5194/acp-13-9565-2013.

Yulaeva, E., J. R. Holton, and J. M. Wallace (1994), On the cause of the annual cycle in tropical lower-stratospheric temperatures, *J. Atmos. Sci.*, *51*, 169–174.